Available online at www.sciencedirect.com
ScienceDirect
Journal of Hazardous Materials 143 (2007) 156–170
Journal of Hazardous Materials
www.elsevier.com/locate/jhazmat

Application of multiphase transport models to field remediation by air sparging and soil vapor extraction

M.E. Rahbeh [a], R.H. Mohtar [b,*]

[a] Department of Renewable Resources, University of Alberta, Edmonton, Alberta, Canada
[b] Department of Agricultural Engineering, Purdue University, 225 South University Street, West Lafayette, IN, United States

Received 13 September 2004; received in revised form 26 June 2006; accepted 4 September 2006
Available online 9 November 2006

Abstract

The design and operation of air sparging and soil vapor extraction (AS/SVE) remediation systems remains in large an art due to the absence of reliable physically based models that can utilize the limited available field data. In this paper, a numerical model developed for the design and operation of air sparging and soil vapor extractions systems was used to simulate two field case studies. The first-order mass transfer kinetics were incorporated into the model to account for contaminant mass transfer between the water and air (stripping), NAPL and water (dissolution), NAPL and air (volatilization), and water and soil (sorption/desorption), the model also accounted for soil heterogeneity. Benzene, toluene, ethyl benzene and xylenes (BTEX) were the contaminants of concern in both case studies. In the second case study, the model was used to evaluate the effect of pulsed sparging on the removal rate of BTEX compounds. The pulsed sparging operation was approximated assuming uniform contaminant redistribution at the beginning of the shut-off period. The close comparison between the observed and simulated contaminant concentration in the aqueous phase showed that the approximation of the pulsed sparging operation yielded reasonable prediction of the removal process. Field heterogeneity was simulated using Monte Carlo analysis. The model predicted about 80–85% of the contaminant mass was removed by air–water mass transfer, which was similar to the average removal obtained by Monte Carlo analysis. The analysis of the removal/rebound cycles demonstrated that removal rate was controlled by the organic–aqueous distribution coefficient K_{oc}. Due to the lack of site-specific data, the aerobic first-order biodegradation coefficients (k_{bio}) were obtained from a literature survey, therefore, uncertainty analysis of the k_{bio} was conducted to evaluate the contribution of the aerobic biodegradation to total contaminant removal. Results of both case studies showed that biodegradation played a major role in the remediation of the contaminated sites.

Keywords: Air sparging; Biodegradation; Pulsed sparging; Mass transfer; Field remediation

1. Introduction

The introduction of the Comprehensive Environmental Response, Compensation, and Liability Act (CERCLA) of 1980 [1] created the need for the evaluation and treatment of contaminant plumes caused by accidental spills of industrial waste. The need for multiphase flow and transport models became even more pressing after the development of remediation techniques that require the injection of remedial fluids such as co-solvents, or techniques that involve remediation by advective air flux such air sparging (AS) and/or soil vapor extraction (SVE).

Multiphase flow and transport modeling is a well-known practice in the petroleum engineering, however, the different motivation of the petroleum and environmental engineering promoted the development of models that are generally aimed at the characterization of the contaminant plume [2–5], and the simulation and design of remediation systems [6–10]. Abriola and Pinder [11] demonstrated their model [2] by modelling the one-dimensional hypothetical infiltration of a hydrocarbon mixture into a soil column. Sleep and Sykes [12] considered a hypothetical distribution of organic contaminant in the subsurface. Baehr and Corpcioglu [13] used a one-dimensional approximation to evaluate, hypothetically, the transport of organic contaminant from the unsaturated zone into ground water. Unger et al. [8] and Rathfelder et al. [10] applied their models to hypothetical AS/SVE problems. All of these models and research articles provided an excellent discussion and insight for the numerical

* Corresponding author. Tel.: +1 765 494 1791; fax: +1 765 496 1115.
E-mail address: mohtar@purdue.edu (R.H. Mohtar).

0304-3894/$ – see front matter © 2006 Elsevier B.V. All rights reserved.
doi:10.1016/j.jhazmat.2006.09.098

solution of multiphase systems, however, without application to field case studies, Radideau et al. [14] and Benner et al. [15] applied semi-empirical models to field case studies. Semi-empirical models, however, require an on-site pre-calibration of an existing air sparging system before it can be used. In this case, the model cannot be used for the design and feasibility studies, and cannot be used for short-term operations, which may defeat the purpose of the model in the first place.

Our objective is to demonstrate the use of a practical and efficient model in the evaluation of two AS/SVE field case studies. The main advantage of the model is its flexibility to take advantage of the limited amount of data that are usually available, while retaining the ability to simulate the processes that contribute to the overall contaminant removal. The analysis for the first case study focuses on the effect of natural attenuation on the contaminant removal processes. The second case study addresses the issues of heterogeneity and pulse sparging, a technique that is usually used to enhance the performance of AS systems.

2. Methodology

2.1. Model description

The unsaturated air flow and contaminant transport model uses first-order kinetics to represent the mass transfer among the aqueous, gaseous, solid, and NAPL phases. The model accounts for heterogeneous domains and considers distinguished single-phase and multi-phase domains. This capability is especially important in the case of remediation techniques that involve an advective air flux such as air sparging and soil vapor extraction. In such systems, two domains may be considered, the advective domain, i.e. the air, and the non-advective domain, which may be either the domain outside the advective air domain but in the vicinity of the air-plume, or any space or pocket inside the advective air domain that is not in direct contact with the advective air domain. The model consists of two main modules; the first module, the steady state unsaturated flow that solves for air flow, uses air permeability as an input and determines the capillary pressure head distribution. The flow module can consider air injection (air sparging) by imposing positive pressure as a fixed boundary condition at the sparging well. Likewise, negative pressure can be imposed to represent extraction (SVE). The second module, multiphase contaminant transport, incorporates first-order mass transfer kinetics to model the contaminant mass transfer among all phases involved: namely, the aqueous, gaseous and, solid phases. The flow and transport simulations are decoupled such that the steady state air flow is determined first, and then the pressure heads are interpolated to the transport model.

2.1.1. The steady unsaturated flow module

AS and/or SVE are usually applied to remove trace and residual contaminant concentrations rather than removing the NAPL free phase. In practice neither free flowing light non-aqueous (LNAPL) nor dense non-aqueous phase (DNAPL) have been detected at sites where an advective air flux technology has been used as a remediation technique [16,17]. Furthermore, it has been found that the effect of ground water flow on the size and shape of ROI is negligible [18], and that the time required for an AS to reach steady state is negligible relative to the average operational time [16,18]. For SVE applications, Massmann [19] treated the air flow as saturated, i.e. single phase flow, by ignoring the effect of the soil moisture condition in the vadose zone. Sawyer and Kamakoti [20], realizing the analogy between flow equations, went one step further and used MODFLOW as a design tool for SVE systems. In this paper, we used the unsaturated steady state flow model SPARG, developed by Mohtar et al. [21], to supplement the transient multiphase model. This involved the assumption of instantaneous attainment of the steady state conditions, which may incur some error at the beginning of simulation. However, it allowed independent simulation for the transport and flow components, thus saving substantial effort and computational time.

2.1.2. Multiphase transport module

The multiphase contaminant transport model uses first-order mass transfer kinetics, $\mathrm{d}C/\mathrm{d}t = k_{\mathrm{f}}(C - C_{\mathrm{aq}})$, to represent mass transfer among the aqueous, gaseous, solid and NAPL phases. The theoretical basis of the multiphase transport model is founded on the concept that a polar liquid wets a polar surface in preference to non-polar liquid, therefore, water preferentially wets soil particles, thus preventing a direct contact between the soil particles and intruding non-aqueous phase or advecting gaseous phase. This has been demonstrated by Wilson et al. [22] using etched glass micro models to visualize the distribution of non-aqueous phase liquid (NAPL), water and air phases. They concluded that the glass was always surrounded by a thin film of water as the air and water were in contact with each other, but not with the glass which represented the soil particle in an actual porous medium. Therefore, the contaminant mass transfer can take place across the aqueous–solid (sorption/desorption), aqueous–gaseous (stripping), aqueous–NAPL (dissolution), and gaseous–NAPL (volatilization) interfaces. In the context of remediation by AS/SVE, the mobile phases may be restricted to the aqueous and gaseous phases only. However, the model incorporates a seepage process in terms of a first-order sink term in order to relax the stationary aqueous phase assumption, and to compensate for the contaminant movement due to the gentle slope in the water table.

2.1.3. Governing equations

The governing equations are based on the concept of conservation of mass and volume averaging, or the representative equivalent volume (REV) [23], which has been extensively used in multiphase contaminant transport models including those involving an advective gaseous phase.

Accordingly, the governing equation for the contaminant transport in the aqueous phase is written as (e.g., Fetter [24]):

$$\frac{\partial C^{\alpha}_{\mathrm{aq}}}{\partial t} = \nabla J^{\alpha}_{\mathrm{aq}_i} - R^{\alpha}_{\mathrm{stripping}} - R^{\alpha}_{\mathrm{soprtion/desorption}} + R^{\alpha}_{\mathrm{dissolution}} - \kappa C^{\alpha}_{\mathrm{aq}} - \beta C^{\alpha}_{\mathrm{aq}}, \quad i = 1, 2 \tag{1}$$

where i denotes the space dimension; α the contaminant type; C_{aq} the contaminant concentration in the aqueous phase (M/L^3); J_{aq} the contaminant flux in the aqueous phase (M/L^{2}T); $R_{stripping}$ the rate of mass transfer per unit volume per unit time across the aqueous–gaseous interface (M/L^{3}T); $R_{sorption/desorption}$ the rate of mass transfer per unit volume per unit time across the aqueous–solid interface (M/L^{3}T); $R_{dissolution}$ the rate of mass transfer per unit volume per unit time across the aqueous–NAPL interface (M/L^{3}T); κ the first-order bio-decay coefficient (1/T); β represents the seepage process as the first-order sink term (1/T).

The governing equation for the contaminant in the gaseous phase is written as

$$\frac{\partial c_g^\alpha}{\partial t} = \nabla J_{g_i}^\alpha + \frac{S_{aq}}{S_g} R_{stripping}^\alpha + R_{volatilization}^\alpha, \quad i = 1, 2 \tag{2}$$

where c_g is the contaminant concentration in the gaseous phase (M/L^3); J_g the contaminant flux in the gaseous phase (M/L^{2}T); S_{aq} the saturation of the aqueous phase (unitless); S_g the saturation of the gaseous phase (unitless); $R_{volatilization}$ is the rate of mass transfer per unit volume per unit time across the gas–NAPL interface (M/L^{3}T).

The governing equation for the contaminant on the solid phase is written as

$$\frac{\partial S_s^\alpha}{\partial t} = \frac{\eta S_{aq}}{\rho_b} R_{sorption/desorption}^\alpha \tag{3}$$

where S_s is the contaminant content in the solid phase (M/M); η the porosity of the solid phase (unitless); ρ_b is the soil bulk density (M/L^3).

The governing equation for the contaminant in the NAPL phase is written as

$$\frac{\partial X_{NAPL}^\alpha}{\partial t} = -\frac{S_{aq}}{\theta_{NAPL}\rho_{NAPL}} R_{dissolution}^\alpha - \frac{S_g}{\theta_{NAPL}\rho_{NAPL}} R_{volatilization}^\alpha \tag{4}$$

where X_{NAPL} is the non-aqueous phase volumetric fraction (unitless); θ_{NAPL} the non-aqueous phase initial residual saturation (unitless); ρ_{NAPL} is the density of the non-aqueous phase (M/L^3).

The governing equation for the contaminant flux in the aqueous phase is written as

$$\nabla J_{aq}^\alpha = \frac{\partial}{\partial x_i}\left(D_{aq_i}^\alpha \frac{\partial C_{aq}^\alpha}{\partial x_i}\right), \quad i = 1, 2 \tag{5}$$

where D_{aq} is the aqueous phase diffusion coefficient (L^2/T).

The governing equation for the contaminant flux in the gaseous phase is written as

$$\nabla J_g^\alpha = -v_g \frac{\partial c_g^\alpha}{\partial x_i} + \frac{\partial}{\partial x_i}\left(D_{g_i}^\alpha \frac{\partial c_g^\alpha}{\partial x_i}\right), \quad i = 1, 2 \tag{6}$$

where v_g is the velocity of the advective gaseous phase (L/T); D_{g_i} is the hydrodynamic dispersion coefficient of the gaseous phase (L^2/T).

The mass transfer stripping term is written as

$$R_{stripping}^\alpha = k_s\left(C_{aq}^\alpha - \frac{c_g^\alpha}{K_H^\alpha}\right) \tag{7}$$

where k_s is the aqueous–gaseous first-order mass transfer coefficient (1/T); and K_H is the dimensionless Henry's coefficient.

The mass transfer sorption/desorption term is written as

$$R_{sorption/desorption}^\alpha = k_d\left(C_{aq}^\alpha - \frac{S_s^\alpha}{K_D^\alpha}\right) \tag{8}$$

where k_d is aqueous–solid the first-order mass transfer coefficient; and K_D is the aqueous–solid distribution coefficient; it is a function of organic fraction (f_{oc}), and organic–aqueous distribution coefficient K_{oc}; $K_D = f_{oc}K_{oc}$ (L^3/M).

The mass transfer dissolution term is written as

$$R_{dissolution}^\alpha = k_{dis}(\chi_{naq}^\alpha \mathrm{Sol}^\alpha - C_{aq}^\alpha) \tag{9}$$

where k_{dis} is the NAPL–aqueous first-order mass transfer coefficient (1/T); χ_{naq} the contaminant molar fraction within the NAPL composite (unitless); Sol is the solubility limit of the contaminant in the aqueous phase (M/L^3).

The mass transfer volatilization term is written as

$$R_{volitalization}^\alpha = k_v(\chi_{naq}^\alpha \mathrm{Vol}^\alpha - c_g^\alpha) \tag{10}$$

where k_v is the NAPL–gas first-order mass transfer coefficient (1/T); Vol is the equilibrium gaseous contaminant concentration (M/L^3) referred to in this paper as volatility.

Accordingly, the aqueous–gaseous (stripping) first-order mass transfer coefficient is written as [25]:

$$k_s = 10^{-2.49} D_{mg}^{0.16} v_g^{0.84} d_{50}^{0.55} K_H^{-0.61} \tag{11}$$

where D_{mg} is the diffusion coefficient of specific contaminant in the gaseous phase and d_{50} is the mean particle size (L).

The NAPL–air (volatilization) first-order mass transfer coefficient is written as [26]:

$$k_v = 10^{-0.42} D_{mg}^{0.38} v_g^{0.62} d_{50}^{0.44} \tag{12}$$

The first-order NAPL–water (dissolution) mass transfer coefficient is written as [27]:

$$k_{dis} = 10^{-2.69} D_{maq}^{1} v_{aq}^{0.60} d_{50}^{-0.73} \tag{13}$$

where D_{maq} is the diffusion coefficient of specific contaminant in the aqueous phase and v_{aq} is the water velocity (L/T).

The solid–aqueous (sorption/desorption) first-order mass transfer coefficient can be determined using the linear regression suggested by Brusseau and Rao [28]:

$$\log k_d = 0.301 - 0.668 \log k_D \tag{14}$$

The current model incorporates air flow and contaminant transport processes. The numerical code for the air flow distribution is derived from SPARG model developed by Mohtar et al. [21]. Their model is based on a steady state unsaturated flow equation of the form:

$$\nabla\left(\frac{k_p k_{rg}(P_c)}{\mu_g}\nabla(P_c - \Delta\rho g Z)\right) = 0 \tag{15}$$

where k_p is the intrinsic permeability (L^2); k_{rg} the gaseous phase relative permeability (unitless); μ the viscosity ($M/L/T^2$); P_c the capillary pressure head ($M/L/T^2$); ρ the density (M/L^3); $\Delta\rho = \rho_{aq} - \rho_g$; g the acceleration of gravity (L/T^2); Z is the elevation head (L); and the subscripts 'aq' and 'g' denote the aqueous and gaseous phases, respectively. The pressure–permeability relationship is governed by the Brooks and Corey [29] equation:

$$k_{rg} = \left(1 - \left(\frac{P_d}{P_c}\right)^{\lambda}\right)^2 \left(1 - \left(\frac{P_d}{P_c}\right)^{2+\lambda}\right) \quad (16)$$

where P_d is the entry air pressure head ($M/L/T^2$) and λ is the particle size distribution index [29]. Eq. (16) is a non-linear function of P_c since the relative permeability is a function P_c.

A FORTRAN 90/95 code was developed using the finite element Galerkin formulation for spatial integration and central finite difference scheme for time integration to solve for unsaturated air flow and multiphase contaminant transport. The model inputs include initial condition, the chemical properties of the contaminants, and flow parameters. The model output includes the capillary pressure distribution, from which the air flow velocities can be calculated, and the contaminant concentration in all the phases involved. The numerical solutions of partial differential equations (PDE) usually result in sparse matrices; therefore, it is only sufficient to store the non-zero entries. This program stores the system of equations in a single vector, e.g. $\{A\}$. The same routines are used to solve for the flow and transport to ensure efficient usage of storage and computational time. The main modules may be categorized in four major groups: (1) modules to read the problem description, element and nodal information, (2) modules used to determine the size of the system of equations, (3) modules used to compose the system of equations using the finite element-Galerkin's formulation, and (4) modules used to solve the system of equations using the Gauss–Siedel iterative technique, which is particularly suitable for sparse matrices. These categories also signify the four major steps that the program executes when solving either for air flow or multiphase contaminant transport. The possibility is retained that the mesh used for the transport problem may be different from that of the flow problem. In this case, the capillary head distribution resulting from the flow module is interpolated into the transport module using mesh interpolation subroutine. The sequential execution of the model first starts by reading the input data, which then is used to form the global matrix of the unsaturated flow problem. After solving for the flow problem the capillary heads are interpolated into the transport problem mesh, in turn the model forms the system of equations form the transport problem and solves it.

2.2. Pulsed air sparging approximation

The finite element model described above consists of a steady state unsaturated air flow module and a transient contaminant transport module that incorporates first-order mass transfer kinetics to simulate the inter-phase contaminant transfer. To enable the model application to pulsed air sparging, we assume that the mixing that occurs after each on and off cycle will be sufficient to produce uniform contaminant distribution at the beginning of the following cycle, as suggested by Marley et al. [30]. Thus, in addition to ignoring the transient stage of air flow distribution, another error is incurred by ignoring the transient stage of the contaminant redistribution in the aqueous phase following the collapse of the radius of influence (ROI) of the air-plume. The assumption is advantageous, however, because it allows easy simulation of pulsed air sparging systems using limited available field data. The validity of the assumption will be assessed by whether or not the model is capable of predicting the contaminant removal within acceptable bounds of error, or within the field data measurement error. The simulation starts with an evenly distributed aqueous concentration at the beginning of the air sparging cycle. At the beginning of the off cycle, the remaining contaminant mass is redistributed evenly in the zones that originally contained the contaminant within the ROI. During the off cycle, changes in the contaminant profile occur due to microbial and mass transfer process such as sorption/desorption, and dissolution. The redistribution of the contaminant depends on the permeability of the flow field. The higher the permeability, the better is the redistribution and mixing of the displaced water. AS/SVE systems are usually used to remediate permeable soils, thus, the approximation of pulsed air sparging as discussed above is applicable under the conditions that are favorable to contaminant removal by an advective air flux.

3. Air sparging case studies

3.1. Porter County

The study area is located in northern Porter County, Indiana near the southern shore of Lake Michigan. The site was utilized by a tin plate manufacturer; a small area of about 220 m^2 was used from 1980 till about 1987 as a drum storage area (DSA) for wastes and organic chemicals used for the cleaning and maintenance of tin plate sheets, mainly light LNAPL with a density of approximately 0.85 g/cm^3. The major constituents included acetone (2-propanone), 2-butoxyethonal, 2-ethoxyethyl acetate, methyl ethyl ketone (2-butanone), petroleum naphtha, toluene, and xylenes. The site became under scrutiny during the closure of the DSA; high levels of substituted benzenes, polycyclic aromatic hydrocarbons, alkanes, and cycloalkane were identified. Additional soil and ground water investigations were undertaken to determine the extent of the contamination [31].

The study revealed that the soil and groundwater under the former DSA contained xylenes, toluene, ethyl benzene, and naphthalene, and 2-mehylnaphthalene. The TEX compounds were detected with regularity in the ground water. The toluene and xylene were above the EPA standard of MCL as shown in Table 1. Therefore, the numerical analysis will be conducted for xylenes and toluene only.

Soil samples were obtained from several depths beneath the former DSA, which indicated that the extent of contamination was to a depth of about 3 m. The contaminants in some of the soil samples exceeded the equilibrium concentrations indicated by

Table 1
The toluene, ethyl benzene and xylenes concentration in ground water on November 1991 (Porter County) [31]

Compound	Concentration (ppm)	MCL (ppm) EPA standard
Toluene	1.1	1
Xylene	18	10
Ethyl benzene	0.16	0.70

the soil–water equilibrium distribution coefficient, $S_s = K_D C_{aq}$, assuming that the soil and groundwater were already in equilibrium. In addition, some NAPL droplets were recovered from the groundwater downstream of the DSA site indicating the presence of residual NAPL phase [31]. The contaminant distribution among the three existing phases; aqueous, solid and residual NAPL, may be determined by taking the equilibrium partitioning assumption, and adding another assumption which states that the soil sample of the highest concentration represents the initial composition, therefore, it can be used to determine the mole fraction of each contaminant species and its corresponding effective solubility and volatility (effective solubility = X_{naq}^{Sol}) [31]. The presence of residual NAPL phase can be assessed by comparing the effective solubility with the aqueous phase concentration resulting from the equilibrium distribution of the contaminants between soil and water. If the aqueous phase concentration exceeds the effective solubility then the NAPL phase is present. The average contaminant distribution throughout the soil profile of the drum storage area (DSA) site is represented in Table 2, where as Table 3 presents the soil–water distribution coefficients, and the effective solubilities and volatilities of the TEX compounds.

The remediation of the site was carried out using AS/SVE system that consisted of 10 air sparging wells, along with a perforated SVE line. The wells were equally distributed over an area of 360 m^2 resulting in a uniform spacing of 6 m between injections wells. Fig. 1 shows that the injection wells were driven to a depth of 6.0 m below ground surface and approximately 4.5 m below the water table. Fig. 1 also shows the general trend of heterogeneity, which mainly consisted of a layer of peat interbeded with fine sand.

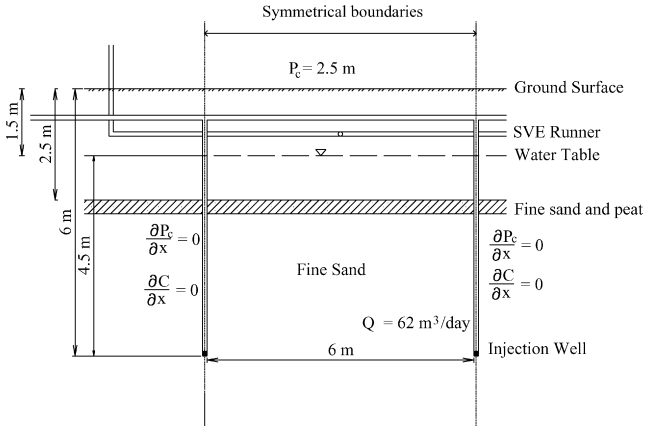

Fig. 1. General characterization of the subsurface and including the modeling domain and the boundary conditions of the Porter County case study.

A small scale-pumping test revealed that the vertical hydraulic conductivity (K) of the unconfined aquifer is on the average of 0.056 cm/s, which translates to an intrinsic permeability (k_p) of 5.09×10^{-11} m^2 ($k_p = K\mu_w/g$, where μ_w is water viscosity and g is the gravitational acceleration). The permeability of the peat layer is incorporated within this value, but remains unknown. Stanford [31] reported, however, that the air was injected at a rate of 0.035–0.051 SCMM (standard cubic meter per minute) per injection well, or an average of 62 m^3/day per injection well. Stanford [31] also conducted several pilot tests and determined that the ROI of the system was about 3 m. Several air flow simulations substituting different intrinsic permeability values for the peat layer showed that the permeability of the sand/peat later should be half of the aquifer's average permeability, which is an intrinsic permeability of 2.5×10^{-11} m^2, in order to produce the aforementioned injection rate and a ROI of about 3 m. The other main soil physical characteristics are listed in Table 4.

Table 2
The average distribution of the TEX compounds in the subsurface on November 1991, Porter County

Compound	Soil concentration (mg/kg)			Residual NAPL (mg NAPL/kg soil)		
	D_1[a]	D_2[a]	D_3[a]	D_1[a]	D_2[a]	D_3[a]
Toluene	0.08	1.76	1.76	0.00	16.24	20.24
Xylenes	38.21	61.20	61.20	0.00	203.60	40.62
Ethyl benzene	0.00	0.54	0.54	0.00	14.78	31.46

Source: Stanford [31].
[a] D_1, D_2 and D_3 are depth intervals of 0.3–0.9 m, 1.1–1.7 m and 2.6–3.2 m, respectively.

Table 3
The soil–water distribution coefficient and, effective solubilities and volatilities of TEX compounds on November 1991, Porter County

Compound	K_D (L/kg)	Solubility (mg/L)	Effective solubility (mg/L)	Volatility (mg/L)	Effective volatility (mg/L)
Toluene	1.6	526.0	3.85	110.88	0.81
Xylenes	3.4	175.0	28.90	88.85	14.67
Ethyl benzene	3.4	206.0	2.30	58.07	0.65

Source: Stanford [31].

Table 4
The input parameters for the Porter County case study

Parameter	Input	Method of determination
Average intrinsic permeability	5.09×10^{-11} m^2	Measured [21]
Peat layer intrinsic permeability	2.5×10^{-11} m^2	Calculated [21]
Sand layer organic fraction	0.006	Measured [31]
Peat layer organic fraction	0.067	Measured [31]
Porosity	29%	Measured [31]
Pore size distribution, λ	3.4	Literature [21]
Entry pressure, P_d	0.2 m	Literature [21]
Grain size, d_{50}	0.020 cm	Measured [31]
Air flow	62 m^3 day^{-1}	Measured [31]
Seepage, $k_{seepage}$	0.068 day^{-1}	Eq. (17)
Xylene, k_{abio}	0.014 day^{-1}	Calculated ($k_{abio} = -\ln(C_{aq}/C_0)v/R$)
Toluene, k_{abio}	0.01 day^{-1}	Calculated ($k_{abio} = -\ln(C_{aq}/C_0)v/R$)
Ethyl benzene, k_{abio}	0.007 day^{-1}	Calculated ($k_{abio} = -\ln(C_{aq}/C_0)v/R$)
Xylene, k_{bio}	0.099 day^{-1}	Literature [32]
Toluene, k_{bio}	0.18 day^{-1}	Literature [32]

Since the air sparging wells were uniformly installed, and the available data only provided an average description of the subsurface and the contaminant distribution, the numerical problem was reduced to two-dimensional symmetrical domain. As shown in Fig. 1, the actual modeling domain consisted of two sparging well and vapor extraction point. The two-dimensional problem domain was assumed to be symmetrical to represent the uniformly spaced AS/SVE sparging system. The flow from a single injection well could be simulated as axisymmetric problem, however, the objective was to approximate the operation of the air sparging remediation system using a subset of two air sparging wells. In addition, the simulation problem included transport and mass transfer process within and outside the air advective zone, thus the Cartesian coordinates were more suitable than the radial coordinates. Besides, the requirements of boundary conditions and region geometry independency of the circumferential direction would invalidate the axisymmetric assumption. Therefore, a two-dimensional cross-sectional domain was retained.

Accordingly, zero flow boundary conditions were imposed on the vertical boundaries to indicate the symmetry. Eq. (15) assumes a static water table and steady state conditions, therefore, a fixed capillary pressure of 1.5 m, a value equal to the depth of the water table below the ground surface, was imposed on the upper boundary, while the lower boundary was treated as infinite. For this condition to hold, the problem domain was doubled in the vertical direction, hence, the overall dimensions of the modeling domain were 6 m × 12 m. As for the transport problem, a zero flux boundary and variable flux boundary conditions were imposed on the side and upper boundaries, respectively. The gas extraction point within the domain was modeled as a sink term. The air flow problem was solved using a uniform mesh of 0.5 m × 0.5 m bilinear elements resulting in total of 264 element and 299 nodes. The same mesh was used to solve for the transient transport problem. As for discretization in time, a time step of 1 day was found suitable in terms of computational time and numerical accuracy and stability.

The system was operated continuously for almost 3 years, from October 1992 to November 1995. During that period the only available monitoring data were from downstream wells. No other soil tests were conducted. The monitoring well was sampled approximately 360 days before and 96 days after the onset of the sparging operation. Neither of these two samples could be taken as an initial condition since the site was subject to anaerobic biodegradation, evident from the emissions of methane gas observed by Stanford [31]. Additionally, seepage (the horizontal flow of ground water out of the contaminated zone) effects could not be ignored as there was a 2.48 m/day average water seepage velocity along the DSA site. Therefore, preliminary runs were performed for a total simulation time period of 360 days, without air sparging, in order to obtain realistic initial conditions. The two main unknowns required for the preliminary run were the seepage loss rate, and the anaerobic decay rate. The seepage was determined from the velocity (v), the soil porosity (η), the cross-sectional area and the contaminated volume [31] as

$$k_{seepage} = \frac{v \times \text{area} \times \eta}{\eta \times \text{volume}} = \frac{2.48 \times 4.5 \times 6.0 \times 0.29}{0.29 \times 12 \times 18 \times 4.5} \approx 0.068\ \text{day}^{-1} \quad (17)$$

The determination of the anaerobic biodegradation coefficient is not as straight forward as the seepage loss rate; nevertheless, approximate estimates were made using available field observations. For instance, none of TEX compounds have been detected in two monitoring wells 20–25 m downstream the main monitoring well, indicating high retardation and an anaerobic degradation. Considering a steady state general approximation, e.g.: $k_{abio} = -\ln(C_{aq}/C_0)v/R$. We note that the k_{abio} is within the range of 0.005–0.02 day^{-1} for any of the TEX compounds. The actual k_{abio} used were 0.014 day^{-1} and 0.01 day^{-1} for xylenes and toluene, respectively. The properties of the TEX compounds are shown in Tables 2 and 3. The rest of the input parameters and their method of determination are shown in Table 4.

The following are the main assumptions made in determining the input parameters:

1. A subset of two wells is representative of the whole site.
2. Water seepage is a function of average velocity and the cross-sectional area of the DSA site.
3. The anaerobic biodegradation coefficients are selected based on the average distance between the DSA and the monitoring wells, utilizing a steady state approximation, and taking the overall mass into consideration: $k_{abio} = -\ln(C_{aq}/C_0)v/R$.
4. The aerobic biodegradation is taken as the upper limit value reported in the literature since Stanford [31] reported high biochemical activity.
5. The air flow distribution was determined using steady state solutions and based on an average flow rate of 62 m^3/day for every injection [31].

Table 5
The contaminated field site characterization, Chesterton County

Depth from surface (m)	Soil description	Water content
0–1.2	Clay and silt	Variable water content
1.2–3.7	Fine sand and silt	Variable soil moisture, with a seasonal perched water table present at a depth of 3.7 m
3.7–3.9	Clay and silt	Variable water content
3.9–13.9	Fine to coarse sand	Variable water content, with a water table present at an average depth of 5.9 m
13.9–14.4	Gray clay, trace silt	Variable water content

Source: Stanford and Manti [33].

3.2. Chesterton County

The site is located at Chesterton Indiana. It housed the administration for town operations including the police and fire departments, as well as the clerk-treasures office. Formerly, the town operated two gasoline and one diesel under-storage tanks (UST). On 15 January 1992, however, a release of gasoline was discovered, which led to the removal of the three USTs. On 15 June 1992 a Corrective Action Plan (CAP) based on several phases of investigation summarized the site characterization and emphasized the gasoline constituent, benzene, ethyl benzene, toluene, and xylenes as the contaminants of interest [33]. The soil profile shown in Table 5 had been characterized based on 30 soil borings, and found to be fairly consistent throughout the site. The soil profile description (Table 5), revealed the existence of two water tables; a perched water table of thickness less than 30 cm located approximately 3.6 m below ground surface, and a true water table located at an average depth of 5.9 m below ground surface (bgs) [33].

The two shallow and deep aquifers are separated from each other by an unsaturated depth of about 2 m in thickness [33].

The two aquifers were impacted by the gasoline spill, however, the extent of contamination on the deep aquifer was much wider than the shallow aquifer. Detailed investigation of contaminant distribution and partition in the soils of the shallow aquifer was not available, therefore, we only conducted numerical modeling for contaminant removal by AS/SVE from the deep unconfined aquifer. Detailed investigation of the soils of the deep aquifer was not available either, however, a few soil samples were collected and analyzed for total hydrocarbon (TPH) content. The results of soil analysis indicated the absence NAPL phase [33]. As for contaminant sorbed on the soil, we assume an initial equilibrium between the soil and aqueous phase. Water

Table 6
The average concentration of BTEX constituents in the aqueous phase, Chesterton County

Chemical constituents	Concentrations (mg/L)
Benzene	4.56
Ethyl benzene	1.76
Toluene	10.93
Xylenes	7.43

Source: Stanford and Manti [33].

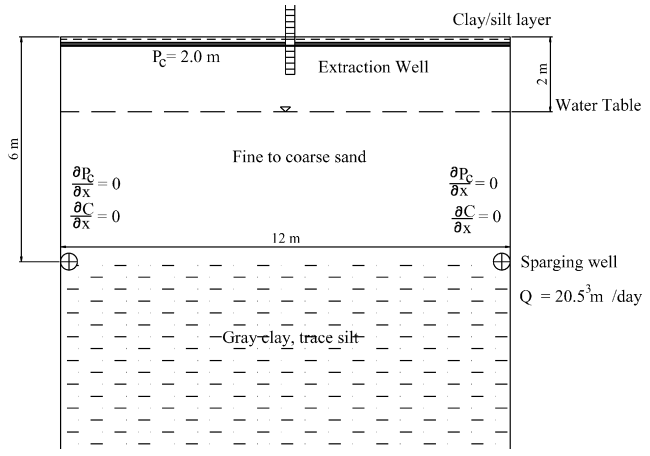

Fig. 2. Cross-sectional area of the subsurface and modeling domain of the Chesterton County case study.

samples were collected from three monitoring wells located around the affected site. Table 6 shows the BTEX constituent concentration for the three monitoring samples on 20 August 1996 prior to the start of AS/SVE operation.

The AS/SVE system consists of 10 sparging wells uniformly distributed at spacing of 12 m; based on radius of influence of about 6 m. As shown in Fig. 2, the AS wells have been driven to a depth of about 6 m (9.75 m bgs) below the semi-impermeable layer separating both aquifers. The soil vapor extraction system consisted of four SVE well drilled to depth of 6.7 m bgs, and installed at uniform distance of 19 m to cover the whole site. Fig. 2, which shows the cross-sectional area of the AS/SVE, also demonstrates the general characterization of the soil profile. It can be noted that the air is injected in the fine sand layer, however, it propagates upward through the more permeable medium sand layer. The air was injected at a rate of 20.5 m^3/day per well. Several air flow simulation substituting different intrinsic permeabilities values showed that an intrinsic permeabilities of 1.5×10^{-11} m^2, and 9.5×10^{-12} m^2 for the medium sand layer and underlying layer, respectively, produce an injection rate of 20.5 m^3/day and radius of influence of about 6 m. Fig. 2 also shows the problem domain, which consisted of a subset of two wells representing the uniformly spaced AS/SVE. Similar to the previous case study, the problem domain was considered symmetrical with zero flow and zero flux conditions imposed on the side boundaries. As necessitated by the assumptions of static water and steady state conditions of Eq. (15), the upper boundary was fixed at capillary pressure of 2 m, i.e. equal to the average depth of the water table. The extraction well was modeled as a sink term. The vertical dimension was doubled to accommodate an infinite lower boundary, thus, the resulting dimensions of the problem domain were 12 m × 12 m. The flow problem was solved numerically using 144 bilinear elements of a grid size of 1 m × 1 m. The same mesh was used for the transient transport problem. A time step of 0.33 day was found to be numerically stable, and was useful in accommodating the pulsed sparging operation.

Pulsed sparging consisted of 8 h of daily operation from 1 September 1996 through March 1999, however, the desired contaminant removal was effectively achieved after 411 days of

Table 7
The values of the first-order bio-decay coefficients considered in the uncertainty analysis

Compound	Lower limit[a] (day^{-1})	Upper limit[a] (day^{-1})	Mean (day^{-1})
Xylenes	0.0019	0.099	0.05
Toluene	0.025	0.18	0.10

[a] *Source*: Suthersan [32].

Table 8
The flow and transport input parameters, Chesterton County

Parameter	Input	Method of determination
Average intrinsic permeability	1.2×10^{-11} m^2	Calculated [21]
Intrinsic permeability sand layer	1.5×10^{-11} m^2	Calculated [21]
Intrinsic permeability clay later	9.5×10^{-12} m^2	Calculated [21]
Pore size distribution index	2.00	Literature [21]
Entry pressure, P_d	0.2 m	Literature [21]
Sand layer organic fraction	0.006	Measured [33]
Porosity	30%	Measured [33]
Grain size, d_{50}	0.025 cm	Measured [33]
Air flow	20 m^3 day^{-1}	Measured [33]
Seepage, $k_{seepage}$	0.00024 day^{-1}	Eq. (18)

the operation. The seepage coefficient was determined from the average seepage velocity of 0.029 m/day [33] and cross-sectional area and the contaminated volume as

$$k_{seepage} = \frac{v \times \text{area} \times \eta}{\eta \times \text{volume}} = \frac{0.029 \times 4 \times 12 \times 0.30}{0.30 \times 1440 \times 4} \approx 2.42 \times 10^{-4}\ \text{day}^{-1} \quad (18)$$

The determination of the anaerobic biodegradation coefficient was approximated from available field observations. Since none of the BTEX compounds were detected in two monitoring wells 60 m downstream from the main monitoring well, then the anaerobic degradation rate, k_{abio} can be determined from steady state general approximation, e.g. $k_{abio} = -\ln(C_{aq}/C_0)v/R$. The flow and transport parameters used in the simulation are shown in Table 7. The determined k_{bio} coefficients and chemical parameters of the BTEX constituents are shown in Table 8.

The assumptions made in determining the input parameters are similar to those employed in Porter County case study, namely:

1. A subset of two wells is a representative to the entire site.
2. Seepage is a function of average velocity and cross-sectional area of the site.
3. The anaerobic biodegradation coefficients are selected based on the average distance between the site and the monitoring wells, utilizing a steady state approximation, and taking the overall mass into consideration.
4. The air flow distribution was determined using steady state solutions and based on an average flow rate of 20.5 m/day for every injection [33].
5. Initial equilibrium exists between the soil and aqueous concentrations.

4. Results and discussion

4.1. Porter County case study

The results of the simulation of the remediation process for a total time period of 1113 days are shown in Fig. 3. The model simulations corresponded very well with the field observed data; this was true for the general case that considers stripping and volatilization by advective air, aerobic and anaerobic biochemical transformation, and seepage, as means of contaminant removal from the subsurface of the former DSA site. However, two additional simulations were taken into consideration to demonstrate the effect or contribution of each of these processes. The first simulation considered the removal by stripping and volatilization only, while the second simulation considered biochemical transformation beside stripping and volatilization. Fig. 3 shows that the removal by stripping and volatilization consisted of two stages. The first stage was the initial stage characterized by rapid removal from the air sparging zone of influence (ROI) and controlled by the first-order mass transfer coefficient (k_s). Following the initial stage was the tailing stage. The contaminant movement and removal during this stage was controlled by slow diffu-

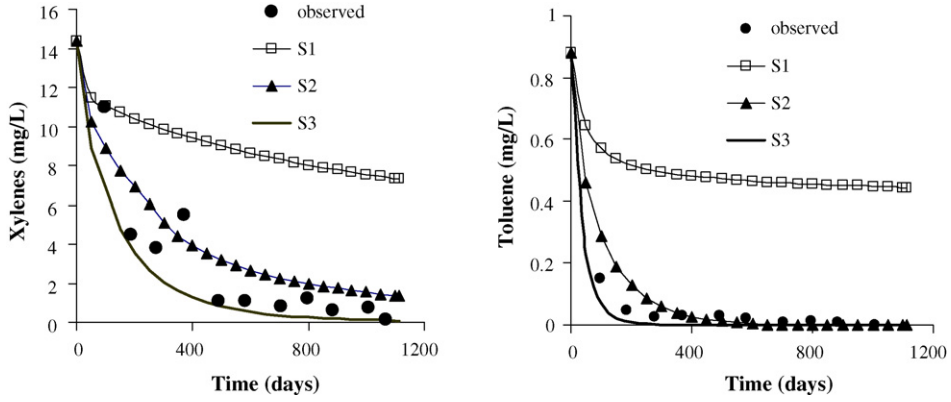

Fig. 3. The comparison between the model simulations and the observed concentrations obtained from a monitoring well located downstream of Porter County site. Where S1 represents the removal by stripping and volatilization, S2 represents stripping, volatilization and biochemical transformation, and S3 represents stripping, volatilization, biochemical transformation and seepage.

sion from outside the zone of influence before it could be stripped from the aqueous phase by the advective air phase. Even if the k_s was increased by several fold this would only accelerate the rapid removal during the initial stage but would not effect on the overall removal time, because the overall removal was limited by the diffusion rates in the aqueous phase. Therefore, for all three TEX compounds air stripping, volatilization were insufficient to account for the contaminant removal.

The model results showed that the main portion of the contaminant was reduced by aerobic biodegradation, which was consistent with field observation of Stanford [31] and Benner et al. [34]. The highest uncertainty; however, came from aerobic biodegradation because the first-order aerobic bio-decay coefficients were not measured or calculated from field observations, but selected from a range of values reported in the literature, not necessarily specific to the site. Therefore, an uncertainty analysis was conducted to assess the effect of this parameter on the model output. Table 7 shows the values used in the analysis, which include the lower and upper limits reported by Suthersan [32] as well as the mean values.

The effect of the aerobic bio-decay coefficients uncertainty on the contaminant removal curve is shown in Fig. 4. For the three TEX compounds, the upper limit of k_{bio} (Table 7) provides a reasonable representation for the aerobic biodegradation. The impact of the k_{bio} reduces as the k_{bio} values increases from the mean to the upper limit. In the case of xylenes, the mean and upper values of k_{bio} produce virtually similar removal curves. This result can be explained by the fact that the aerobic biochemical degradation is limited by oxygen transfer from the gaseous phase into the aqueous phase, therefore, increasing k_{bio} will not necessarily result in a proportional increase in contaminant biodegradation, even when the oxygen threshold is set at zero, i.e. assuming that all dissolved oxygen will be used in aerobic bio-transformation. Adjusting the values of k_{bio} to fit the observed data results in bio-decay rate of 0.08, for xylenes and toluene, which are within the range of values represented in Table 7.

4.2. Chesterton County

4.2.1. Removal processes

The results confirmed previous field observation that only a small fraction the contaminant was removed by stripping and volatilization [33], the rest of the contaminant reduction was attributed to aerobic degradation. In this model, seepage was taken as a sink term because of the limitation imposed by the steady state solution of the air flow distribution, which assumed a stagnant aqueous phase. The seepage was included in all simulations, however, its overall effect was minimal ($k_{seepage} = 2.42 \times 10^{-4}$), therefore, the main focus in this discussion was on the contaminant removal by advective air flux and aerobic biodegradation.

The simulation of the removal of BTEX constituents during air sparging operation was conducted using the input information demonstrated in Tables 8 and 9. The first-order biodegradation coefficient was taken from the literature, and not determined from field observations [29]. Therefore, additional simulations were undertaken using upper and lower limits of k_{bio} to test the effect of the k_{bio} uncertainty on the contaminant removal. The case of physical removal by air stripping without biodegradation was also conducted to demonstrate the relative contribution of each of the removal processes. Fig. 5 shows the comparison between the observed average aqueous concentrations and the simulated results for the removal of benzene, toluene, ethyl benzene, and xylenes, respectively.

The results suggested that the uniform redistribution of the remaining contaminant mass was a satisfactory approximation to predict the contaminant removal during pulsed air sparging. As demonstrated in Fig. 5, the model was able to predict the removal time for the TEX compounds, however, it underestimated the removal time of benzene. The simulated results suggested that at least a portion of the contaminant was biodegraded. The k_{bio} value influenced the removal curves to various degrees. The simulated removal curves using the lower limit values of k_{bio} were comparable with observed data in the case of toluene and ethyl benzene, while in the case of xylene the mean value of k_{bio}

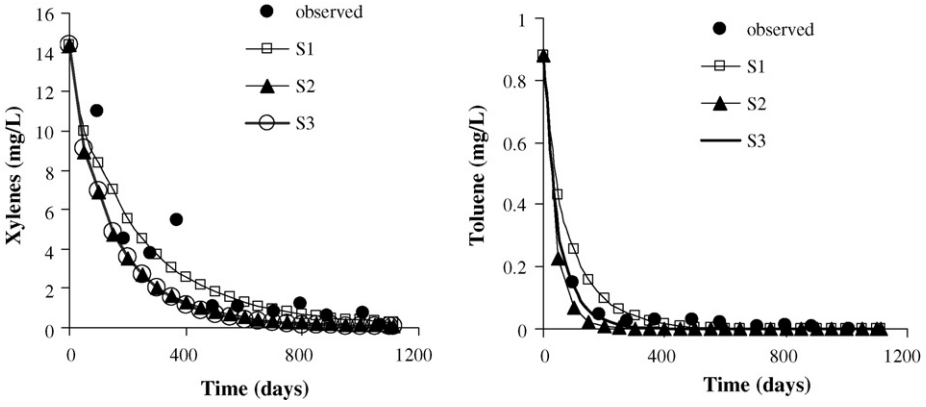

Fig. 4. The results of the uncertainty analysis of the first-order aerobic bio-decay coefficient (Porter County). The observed concentration obtained from a monitoring well located downstream of Porter County site and the model simulation. Where S1 represents the lower limit k_{bio}, S2 represents the upper limit k_{bio}, and S3 represents the average k_{bio}.

Table 9
The physiochemical properties of the organic compounds used in the analysis (Chesterton County)

Property	B[a]	T[a]	EB[a]	X[a]
Molecular weight (g)	78.11[b]	92.1[b]	106.2[b]	318.5[b]
Density (g/cm^3)	0.88[b]	0.87[b]	0.87[b]	0.86[b]
Henry's coefficient (unitless)	0.23[c]	0.27[c]	0.32[c]	0.28[c]
Solubility (mg/L)	1750[c]	526[b]	206[b]	175[c]
Vapor pressure (mm Hg)	75	22[b]	6.9	5.1[b]
Volatility (mg/L)	320.4[d]	110.9[d]	40.07[d]	88.85[d]
Organic constant K_{oc} (L/mg)	58.9[c]	182[c]	363[c]	386[c]
Air diffusion coefficient (m^2 day^{-1})	0.76[e]	0.69[e]	0.64[e]	0.36[e]
Water diffusion coefficient ($\times 10^{-5}$) (m^2 day^{-1})	9.26[f]	8.34[f]	7.67[f]	4.00[f]
Anaerobic biodegradation k_{abio} ($\times 10^{-3}$) (day^{-1})	1.9[g]	5.7[g]	4.3[g]	4.9[g]
Mean aerobic biodegradation, k_{bio} (day^{-1})[a]	0.07 [29]	0.10 [29]	0.15 [29]	0.05 [29]
Lower aerobic biodegradation, k_{bio} (day^{-1})	0.04 [29]	0.025 [29]	0.069 [29]	0.0019 [29]
Higher aerobic biodegradation, k_{bio} (day^{-1})	0.09 [29]	0.18 [29]	0.23 [29]	0.099 [29]

[a] B, benzene; T, toluene; EB, ethyl benzene; X, xylenes; CTC, carbon tetra chloride; CB, chlorobenzene; TCE, trichloroethylene.
[b] Retrieved from www.chemfinder.com.
[c] EPA Soil screening guide.
[d] Calculated as (Fetter [24]): volatility = (vapor pressure (atm) × MW (gm/mol))/(0.0821 atm L/mol K × 293 K)).
[e] Calculated as (Schwarzenbach et al. [35]): $D_a = 10^{-3}[T^{1.75}((1/m_{air}) + (1/m_o))^{1/2}/P(\bar{V}_{air}^{1/3} + \bar{V}_o^{1/3})^2] \times 10^{-4} \times 3600 \times 24$; where D_a is the air diffusion coefficient (m^2/day); T the absolute temperature (K); m_{air} the average molecular mass of air (29 g/mol); m_o the molecular weight of the organic compound (g/mol); P the gas phase pressure (1 atm); $\bar{V}_{air}$ the average molar volume of the gases in air (~20.1 cm^3/mol); $\bar{V}_o$ is the molar volume of the organic compound (cm^3/mol).
[f] Calculated as (Schwarzenbach et al. [35]): $D_m = (0.0001326/\mu^{1.14}(\bar{V}_o)^{0.589}) \times 10^{-4} \times 3600 \times 24$; where D_m is the water diffusion coefficient (m^2/day); μ the water viscosity (0.894 centipoise); $\bar{V}_o$ is the molar volume of the organic compound (cm^3/mol).
[g] $k_{abio} = -\ln(C_{aq}/C_0)v/R$.

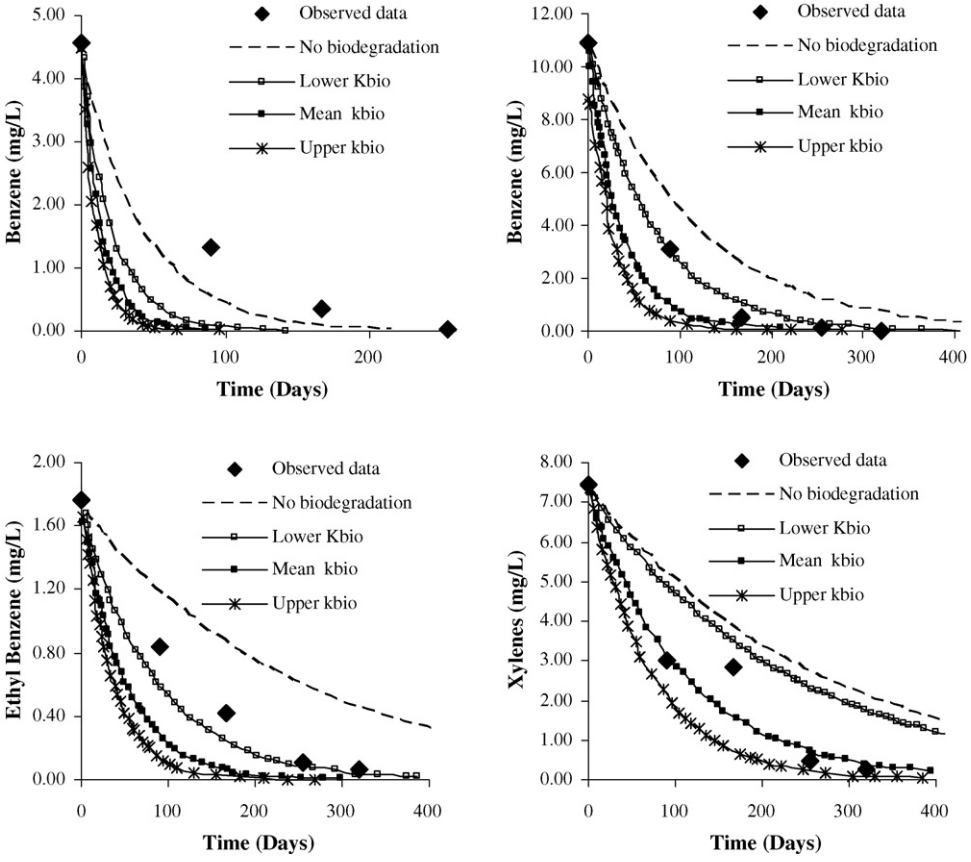

Fig. 5. Comparison between the simulated removal and the average BTEX concentration observed for three sampling well located with the Chesterton County site.

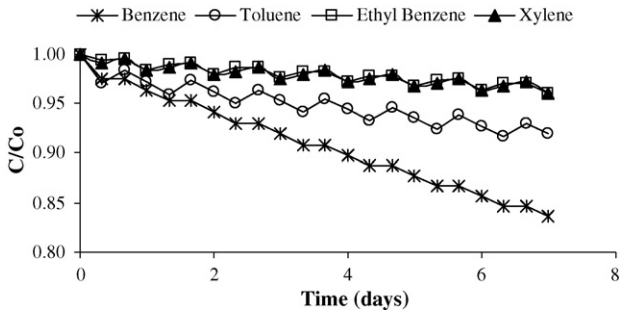

Fig. 6. The removal/rebounds cycle of the BTEX constituents during the first week of operation (Chesterton County).

seemed appropriate, thus, the first-order aerobic biodegradation for toluene, ethyl benzene, and xylenes range from 0.025 to 0.05 day^{-1}. However, using any of the three k_{bio} values, over predicted benzene removal, which could be inferred as the absence of the microbial degraders or due to low biodegradation in this site as indicated by the results of toluene, ethyl benzene, and xylenes.

These results are confirmed by the results obtained by Benner et al. [15] who calibrated a low biodegradation coefficients values for the same site. Also, it should be noted that the K_{oc} of benzene is relatively lower than the other three BTEX compounds. Subsequently, benzene sorption/desorption process is slower than the other BTEX compounds, thus, the stripping and aerobic biodegradation dynamics are faster than the rest of the of the BTEX compounds. Faster dynamics are more difficult to predict, therefore, more discrepancies are expected. More detailed discussion about the effect of the K_{oc} values on the BTEX removal mechanisms follows.

4.2.2. Contaminant removal/rebound cycles

Contaminant removal and rebound curves were observed from the model results within each cycle. Fig. 6 shows the removal/rebound cycles of each of the BTEX constituents during the first week of operation. Benzene demonstrated the faster removal and the lowest rebound, while ethyl benzene and xylenes demonstrated the slowest removal and the highest rebound, which explains the fast benzene removal, and slow ethyl benzene and xylene removal are shown in Fig. 5. Figs. 7–10 show the fluctuations of the BTEX compounds in the aqueous and solid phases. Benzene concentration in the aqueous and solid phases is characterized by a fast removal cycle followed by a recession period without apparent rebound (Fig. 7). Fig. 7 also shows that benzene biodegradation accelerates the contaminant removal from the aqueous phase, which increases the concentration gradient between the aqueous and solid phases, subsequently increasing desorption. As a result, more contaminant mass is removed from both phases. Figs. 8–10 show the removal of toluene, ethyl benzene and xylenes (TEX), respectively, from the aqueous and solid phases during the first week of the operation. The contaminant removal from the aqueous phase exhibited apparent removal and rebound cycles in the aqueous phase, while the solid phase is characterized by a smooth decline

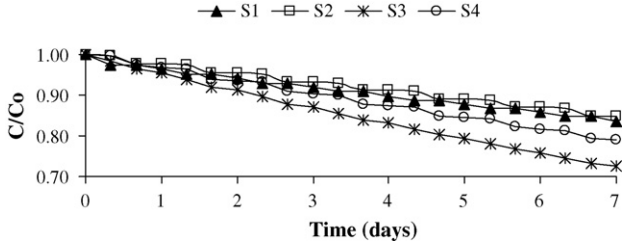

Fig. 7. The removal/rebounds cycle of benzene in the aqueous and solid phase during the first week of operation (Chesterton County). Where S1 represents the removal from aqueous phase using a k_{bio} of 0.0 day^{-1}, S2 represents the removal from the solid phase using a k_{bio} of 0.0 day^{-1}, S3 represents the removal from the aqueous phase using a k_{bio} of 0.04 day^{-1}, S4 represents the removal from the solid phase using a k_{bio} of 0.04 day^{-1}.

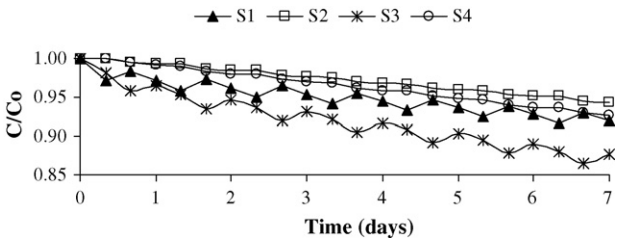

Fig. 8. The removal/rebounds cycle of toluene in the aqueous and solid phase during the first week of operation (Chesterton County). Where S1 represents the removal from aqueous phase using a k_{bio} of 0.0 day^{-1}, S2 represents the removal from the solid phase using a k_{bio} of 0.0 day^{-1}, S3 represents the removal from the aqueous phase using a k_{bio} of 0.025 day^{-1}, S4 represents the removal from the solid phase using a k_{bio} of 0.025 day^{-1}.

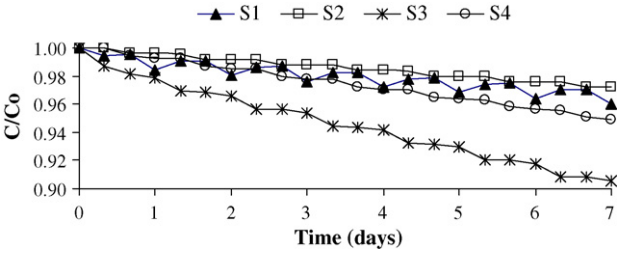

Fig. 9. The removal/rebounds cycle of ethyl benzene in the aqueous and solid phase during the first week of operation (Chesterton County). Where S1 represents the removal from aqueous phase using a k_{bio} of 0.0 day^{-1}, S2 represents the removal from the solid phase using a k_{bio} of 0.0 day^{-1}, S3 represents the removal from the aqueous phase using a k_{bio} of 0.069 day^{-1}, S4 represents the removal from the solid phase using a k_{bio} of 0.069 day^{-1}.

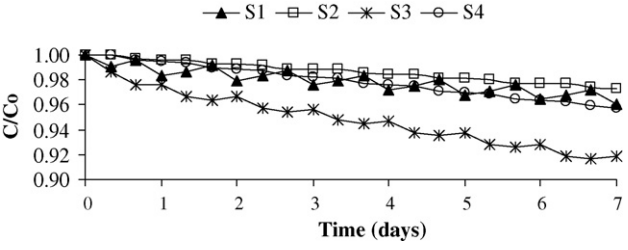

Fig. 10. The removal/rebounds cycle of xylenes in the aqueous and solid phase during the first week of operation (Chesterton County). Where S1 represents the removal from aqueous phase using a k_{bio} of 0.0 day^{-1}, S2 represents the removal from the solid phase using a k_{bio} of 0.0 day^{-1}, S3 represents the removal from the aqueous phase using a k_{bio} of 0.05 day^{-1}, S4 represents the removal from the solid phase using a k_{bio} of 0.05 day^{-1}.

in the contaminant concentration as a result of short release periods, followed by a longer recession period. The release from the solid phase is associated with the rebound in the aqueous phase, which takes place during the shut-off period. During the sparging period, the contaminants are removed from the aqueous phase by stripping. In contrast to benzene, the contaminant mass of TEX in the solid phase remained constant during the sparging period. The aerobic biodegradation curbs the rebound of the TEX compound. This indicates that the aerobic biodegradation proceeds as the contaminant is released slowly to the aqueous phase. The above observations can be summarized as: (1) fast removal of benzene (Fig. 7) from the aqueous phase occurs during the sparging period. Benzene is slowly released into the aqueous phase during the shut-off period, however, without apparent rebound in the aqueous phase. The aerobic biodegradation accelerates the removal from both phases since more desorption occur to compensate for the lost mass in the aqueous phase. (2) The removal of TEX (Figs. 8–10) is characterized by the decrease in the aqueous phase concentration during the sparging period; while the solid phase contaminant concentration remain constant. During the shut-off period the contaminant is slowly released from the solid phase resulting in contaminant rebound in the aqueous phase. Aerobic biodegradation curbs the rebound in the aqueous phase, because the contaminant is degraded as it is slowly released from the solid phase.

The removal/rebound cycle is a function of the Henry's coefficient and air velocity, which influences the water–air mass transfer. Also, it is a function of K_{oc}, which influences the soil–water mass transfer. The air velocity is constant for all contaminants, and Henry's coefficients of the BTEX constituents lie within the same range (Table 9), therefore, the behavior of the removal/rebound cycles described above is actually related to desorption rate which is a function of K_{oc}. According to Table 9, the BTEX constituents can be arranged according to the following order with respect to K_{oc} value: xylene > ethyl benzene > toluene > benzene. This order is also reflected in the removal/rebound cycles shown in Fig. 6, as well as the removal curves shown in Fig. 8. This is because the retardation factor increases as the K_{oc} increases, therefore, for benzene fast desorption occurs as the contaminant is removed from aqueous phase. The unapparent redound of benzene in the aqueous phase can be explained in view of the low K_{oc}. A low K_{oc} means that the equilibrium distribution coefficient is also low ($K_D = K_{oc} f_{oc}$ where f_{oc} is the organic fraction). Therefore, the contaminant amount required to be retained or released from or to the solid phase in order to retain equilibrium is also small, and does not result in high aqueous concentration. In addition, due to a low K_{oc}, the solid phase will quickly release the benzene mass entering the ROI at the beginning of the shut-off period. Simultaneously, fast desorption occurs outside the ROI, which also contributes

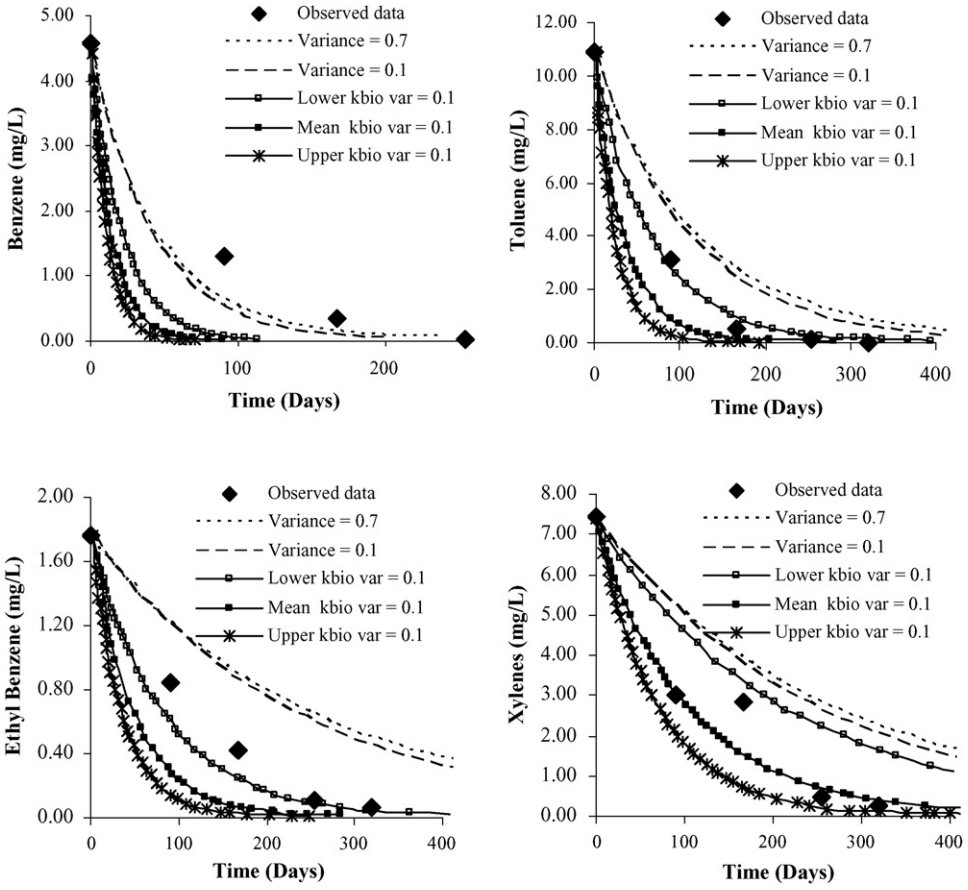

Fig. 11. Monte Carlo average removal curves for: (a) benzene; (b) toluene; (c) ethyl benzene; (d) xylene (Chesterton County).

to nearly constant benzene aqueous concentration during the shut-off period.

4.2.3. Monte Carlo analysis

Monte Carlo analysis was conducted using the mean intrinsic permeability value of 1.2×10^{-11} m^2 indicated from descriptive available field observations (Table 8). However, the information available from field observation was not sufficient to indicate the flow field variance. Therefore, three levels of variances represented by three standard variances (σ^2) of the intrinsic permeability field (k_p); 0.1, 0.3 and 0.7, were used in the analysis. The realization were generated using the turning band method (TBM) as described by Fenton [36]. Initially, the analysis was conducted without biodegradation, however, the effect of aerobic biodegradation was considered using a separate set of realizations. For each realization, the air flow distribution and the BTEX removal was determined using the unsaturated flow and transient flow model. The ensemble average of the results was then obtained to represent the average removal of the BTEX constituents. Fig. 11 shows the average removal from heterogeneous fields of 0.1 and 0.7 variance. In general, Monte Carlo analysis predicted that increasing the heterogeneity would slightly increase the removal time. In fact, the average remaining mass varied only by 2% as the variance increased from 0.1 to 0.7. This difference was not apparent when introducing the effect of bio-degradation, therefore, Fig. 11 only displays the effect of aerobic biodegradation for $\sigma^2 = 0.1$. The comparison between the results of Monte Carlo solution (Fig. 11) and the results of the deterministic model shown in Fig. 5 shows that Monte Carlo analysis and approximate deterministic model provide similar results. The results demonstrate, however, that the Monte Carlo analysis is useful in predicting the average contaminant removal. In the absence of a deterministic characterization flow domain, Monte Carlo can provide an average prediction of the removal processes. Fig. 12 shows four different random realizations of the flow field using the same mean (Table 10) and variance of 0.7, however, the distribution of the low and high permeability zones is different, which is critical for the remediation systems that require an advective air flux. This analysis, however, assumed no spatial correlation, therefore, each Monte Carlo scenario resulted in a fully randomized distribution of the intrinsic permeability which might have attributed to the close resemblance between the deterministic and stochastic solutions. This is because the removal rate is directly affected by the heterogeneity within the ROI. In the context of a Monte Carlo process, this will translate into variable removal rates parallel to the flow field variance. Therefore, increasing the variance will increase the spread around the mean, but will maintain the mean, which will be the same for all variances. The probability density function (pdf) shown in Fig. 13 demonstrates that the probability of the mean varies considerably as the variance increases from 0.1 to 0.7. As shown in Table 10, there is 88% probability that 7.5% of the initial BTEX mass will remain in the subsurface

Table 10
The effect of the variance on the probability of the average contaminant removal

Variance	Probability of the average contaminant removal (%)
0.1	88
0.3	68
0.7	45

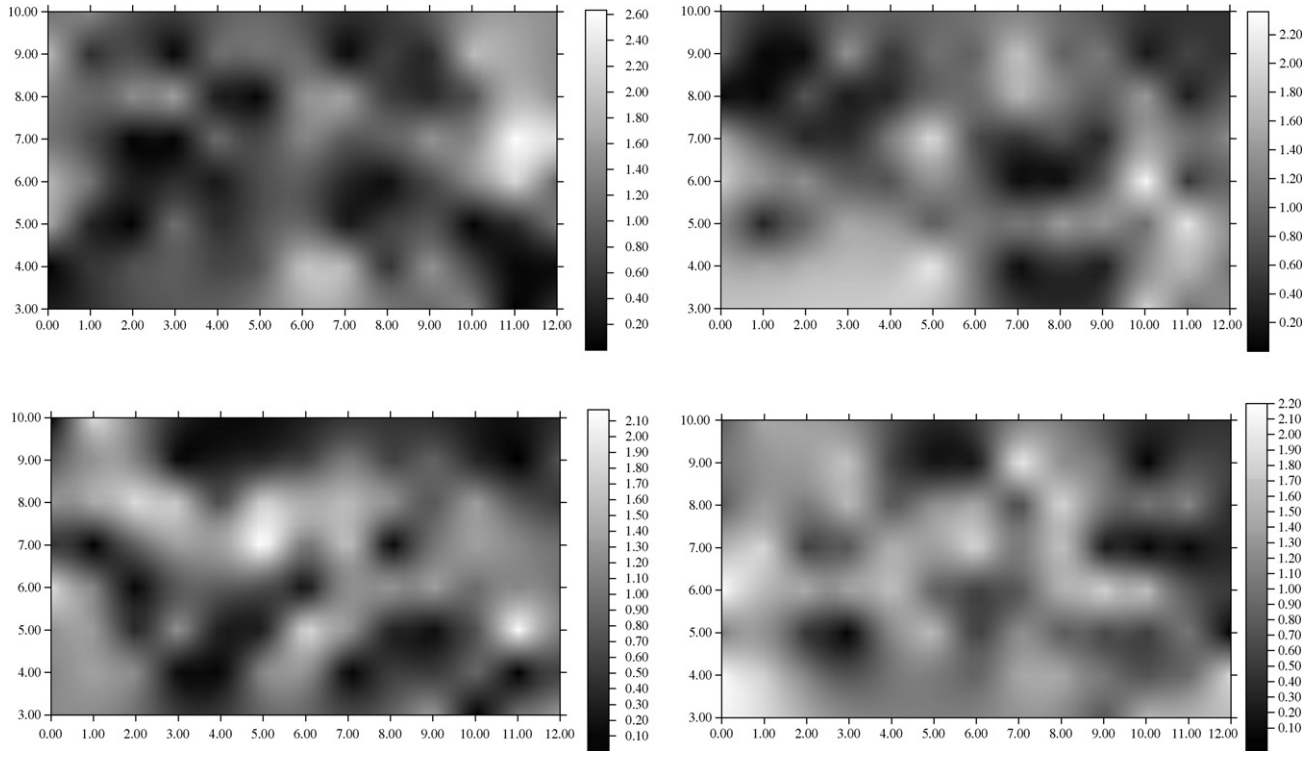

Fig. 12. Four different realization of intrinsic permeability = 1.2×10^{-11} m^2 and variance of 0.7. The grey-color scale is multiplied by 1.2×10^{-11} factor.

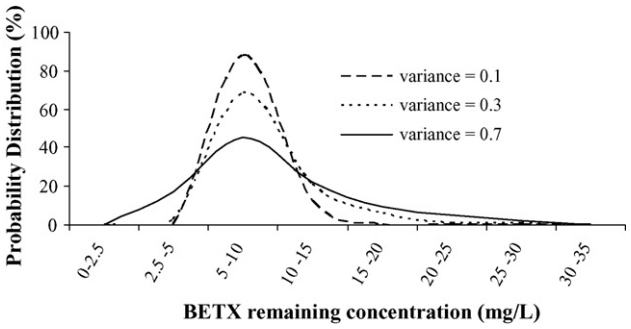

Fig. 13. The probability density function of the percentage of the remaining BTEX contaminant.

at the end of the sparging period. This probability decreases to about 68% and 45% as the variance increases to 0.3 and 0.7, respectively.

5. Conclusions

In this paper, we applied an unsaturated air flow and multiphase contaminant transport model to assess the influence of biodegradation and pulsed sparging on the BTEX removal rate. Two air sparging operations previously conducted in Porter and Chesterton counties of Indiana were simulated. Due to the limited data availability, a symmetrical subset of two well was used to represent the entire field. For both case studies, the contaminant concentration in the ground water was obtained from local monitoring wells within or beside the site in question. An initial equilibrium was assumed between phases in order to obtain the initial contaminant concentration in various phases. All input data, with the exception of first-order aerobic biodegradation coefficients were determined independently from available field observations and the literature. As for the first-order aerobic biodegradation, a range of applicable values was selected from the literature. Uncertainty analysis was then conducted to assess the effect of aerobic biodegradation on the BTEX removal during air sparging. To enable the pulsed sparging simulation, it was assumed that the contaminant redistributed uniformly at the end of each operation period. The simulated results of both case studies were consistent with the observed data.

The simulated contaminant removal of the Porter County case study confirmed previous field observation that only a small fraction the contaminant was removed by stripping and volatilization [31], while the rest of contaminant reduction was attributed to aerobic degradation. Seepage is also an important process that should not be ignored; in this model, seepage was taken as a sink term because of the limitation imposed by the steady state solution of the air flow distribution which assumes a stagnant aqueous phase.

The results of the Chesterton County case study showed close comparison between the simulated and observed results of the BTEX concentration in the aqueous phase, which indicated that the model was able to adequately predict removal of BTEX constituents using pulsed air sparging. This also suggests that the uniform redistribution of the contaminant after each sparging period is a valid assumption. The removal and rebound cycles observed as a result of the AS operation showed that the K_{oc} values play a measurable role in controlling the contaminant removal from the subsurface.

The resemblance between the simulated and the observed results cannot serve as verification for the model because of the assumptions used to evaluate some of the input parameters. Altering any of these assumptions will change the numerical results significantly, although they were predetermined and carefully rationalized. Therefore, detailed monitoring and investigation of the effect of the natural attenuation processes on contaminant removal are essential in order to study the effectiveness of air sparging as remediation technique, and to verify perspective numerical models. The analysis of Porter and Chesterton case studies revealed the importance of the model to assess the contaminant mass removal processes during advective air flux, which can be helpful in the decision and operation of AS/SVE systems in practice.

Acknowledgements

This research was funded by grant form Purdue Research Foundation under grant number PRF 690-1146-3039, and support from Environmental Quality Lab, Department of agricultural and Biological Engineering under award number 6903039. Special thanks to Mr. Steve Stanford of IES Inc. Schererville, Indiana, for providing field remediation reports and consultation during this work.

References

[1] EPA, Soil Screening Guidance: User's Guide, EPA, Washington, DC, 1996.
[2] L.A. Abriola, G.F. Pinder, A multiphase approach to the modeling of porous media contamination by organic compounds. 1: equation development, Water Resour. Res. 21 (1) (1985) 11–18.
[3] M.Y. Corapcioglu, A.L. Baehr, A compositional multiphase model for groundwater contamination by petroleum products. 1: theoretical considerations, Water Resour. Res. 23 (1) (1987) 191–200.
[4] B.E. Sleep, J.F. Sykes, Compositional simulation of groundwater contamination by organic compounds. 1: model development and verification, Water Resour. Res. 29 (6) (1993) 1697–1708.
[5] B.E. Sleep, J.F. Sykes, Modeling the transport of volatile organics in variably saturated media, Water Resour. Res. 25 (1) (1989) 81–92.
[6] M.L. Brusseau, Transport of organic chemicals by gas advection in structured or heterogeneous porous media: development of a model and application to columns experiments, Water Resour. Res. 27 (12) (1991) 3189–3199.
[7] J.E. Armstrong, E.O. Frind, R.D. McClellan, Nonequilibrium mass transfer between the vapor, aqueous, and solid phases in unsaturated soils during vapor extraction, Water Resour. Res. 30 (2) (1994) 355–368.
[8] A.J.A. Unger, Sudicky, P.A. Forsyth, Mechanisms controlling vacuum extraction coupled with air sparging for remediation of heterogeneous formations contaminated by dense nonaqueous phase liquids, Water Resour. Res. 31 (8) (1995) 1913–1925.
[9] J.E. McCray, R.W. Falta, Numerical simulations of air sparging for remediation of NAPL contamination, Ground Water 35 (1) (1997) 99–110.
[10] K.M. Rathfelder, J.R. Lang, L.M. Abriola, A numerical model (MISER) for the simulation of coupled physical, chemical and biological processes in soil vapor extraction and bioventing systems, J. Contam. Hydrol. 43 (2000) 239–270.
[11] L.A. Abriola, G.F. Pinder, A multiphase approach to the modeling of porous media contamination by organic compounds. 2: numerical simulation, Water Resour. Res. 21 (1) (1985) 19–26.

[12] B.E. Sleep, J.F. Sykes, Compositional simulation of groundwater contamination by organic compounds. 2: model application, Water Resour. Res. 29 (6) (1993) 1709–1718.
[13] A.L. Baehr, M.Y. Corapcioglu, A compositional multiphase model for groundwater contamination by petroleum products. 2: numerical solution, Water Resour. Res. 23 (1) (1987) 201–213.
[14] A.J. Radideau, J.M. Blayden, C. Ganguly, Field performance of air-sparging system for removing TCE from groundwater, Environ. Sci. Technol. 33 (1) (1999) 157–162.
[15] M.L. Benner, R.H. Mohtar, L.S. Lee, Factors affecting air sparging remediation systems using field data and numerical simulations, J. Hazard. Mater. B 95 (2002) 305–329.
[16] P.D. Lundegrad, D. LaBrecque, Air sparging in a sandy aquifer (Florence, Oregon, U.S.A.): actual and apparent radius of influence, J. Cont. Hydrol. 19 (1995) 1–27.
[17] D.J. McKay, L.J. Acomb, Neutron moisture probe measurements of fluid displacement during in-situ air sparging, Ground Water Monit. Remediat. (1996) 86–94.
[18] K.R. Reddy, J.A. Adams, Effect of ground water flow on remediation of dissolved-phase VOC contamination using air sparging, J. Hazard. Mater. 72 (2000) 147–165.
[19] J.W. Massmann, Applying ground water flow models in vapor extraction system design, J. Environ. Eng. 115 (1) (1989) 129–149.
[20] C.S. Sawyer, M. Kamakoti, Optimal flow rates and well locations for soil vapor extraction and design, J. Contam. Hydrol. 32 (1998) 63–76.
[21] R.H. Mohtar, L.J. Segerlind, R.B. Wallace, Finite element analysis for air sparging in porous media, Fluid/Particle Sep. J. 9 (3) (1996) 225–239.
[22] J.L. Wilson, S.H. Conard, E. Hagan, W.R. Mason, W. Peplinski, E. Hagan, Laboratory investigation of residual organics, Report CR-813571, U.S. Environmental Protection Agency, Ada, OK, 1990.
[23] M. Hassanizadeh, W.G. Gray, General conservation equations for multiphase systems: 1: averaging procedure, Adv. Water Resour. 2 (1979) 131–144.
[24] C.W. Fetter, Contaminant Hydrogeology, Prentice Hall, Inc., New Jersey, 1999.
[25] K. Chao, S.K. Ong, A. Protopapas, Water-to-air mass transfer of VOCs: laboratory-scale air sparging system, J. Environ. Eng. 124 (11) (1998) 1054–1060.
[26] M.D. Wilkins, L.M. Abriola, K.D. Pennell, An experimental investigation of rate-limited nonaqueous phase liquid volatilization in unsaturated porous media: steady state mass transfer, Water Resour. Res. 31 (9) (1995) 2159–2172.
[27] S.E. Powers, L.M. Abriola, W.J. Weber, An experimental investigation of nonaqueous phase liquid dissolution in saturated subsurface systems: steady state mass transfer rates, Water Resour. Res. 28 (10) (1992) 2691–2705.
[28] M.L. Brusseau, P.S.C. Rao, The influence of sorbate–organic matter interactions on sorption nonequilibrium, Chemosphere 18 (9/10) (1989) 1691–1706.
[29] A.T. Corey, Mechanics of Immiscible Fluids in Porous Media, Water Resources Publications, Littleton, CO, 1986.
[30] M.C. Marley, D.J. Hazebrouck, M.T. Walsh, The application of in-situ air sparging as an innovative soils and groundwater remediation technology, Ground Water Monit. Remediat. 12 (2) (1992) 137–144.
[31] S.M. Standford, Physical and biological effects of in situ air sparging of groundwater contaminated with organic chemicals, M.Sc. Thesis, Purdue University, West Lafayette, IN, 1998.
[32] S.S. Suthersan, Remediation Engineering, Lewis Publishers, Boca Raton, FL, 1997.
[33] S.M. Stanford, S. Manti, SVE and Air Sparging Pilot Study (Pilot Plan), ELF Site 9404534 Remediation, Town of Chesterton, Integrated Environmental Solution Inc., Schereville, Indiana, 1996.
[34] M.L. Benner, S.M. Stanford, L.S. Lee, R.H. Mohtar, Field and numerical analysis of in situ air sparging: a case study, J. Hazard. Mater. 27 (2000) 217–236.
[35] R.P. Schwarzenbach, P.M. Gschwend, D.M. Imboden, Environmental organic chemistry, John Wiley and Sons, Inc., 1993.
[36] G.A. Fenton. Simulation and analysis of random fields, Ph.D. Thesis, Princeton University, Princeton, New Jersey, 1990.